

# SIW Filter Based on a CPW Resonator and a Hybrid Electromagnetic Coupling Structure

Xiaohei Yan, Minjie Guo, Wenjing Mu\*, Xiumei Huang, and Haiyan Zeng

*School of Mathematics, Physics, and Electronic Information Engineering  
Guangxi Minzu Normal University, Chongzuo 532200, China*

**ABSTRACT:** This paper proposes a hybrid cross-coupled filter that utilizes a coplanar waveguide (CPW) resonator and a hybrid electromagnetic coupling structure. The filter features a flexible and controllable position of transmission zeros and a quasi-elliptical response. It is composed of two CPW structures etched within the upper metal surface of a second-order substrate-integrated waveguide (SIW) resonant cavity. By adjusting the dimensions of the two CPW structures between the SIW resonant cavities and the width of the inductive coupling window, the strengths of the electric and magnetic couplings can be easily controlled to achieve a controllable hybrid cross-coupling effect in order to adjust the position of the transmission zeros and ultimately to realize the third-order filter with quasi-elliptical response characteristics. Simulation and test results indicate that the filter has a center frequency of 4.55 GHz, a  $-3$  dB bandwidth of 180 MHz, a relative bandwidth of 4%, an insertion loss of  $-0.9$  dB in the passband, a return loss of over 15 dB, and two transmission zeros located at 4.4 GHz and 4.7 GHz, respectively. The filter has several advantages, including a simple structure, low insertion loss, small circuit size, good frequency selectivity, and flexible and controllable transmission zeros. These features make it suitable for the use in 5G (sub-6 GHz) wireless communication systems.

## 1. INTRODUCTION

Filters are essential in wireless transceiver systems to eliminate noise and maintain radio frequency (RF) system stability, significantly impacting wireless communication transmission quality. Substrate-integrated waveguides have become a popular choice for filter design due to their high-quality factor, low cost, low loss, and easy planar integration [1–6]. With the rapid development of modern microwave and wireless communication systems, hybrid cross-coupling techniques have become widely used in microwave filters to meet performance specifications such as miniaturization, low cost, high selectivity, and strong out-of-band rejection of filters [7–17].

Ref. [7] describes a hybrid electromagnetic coupling method that uses open coplanar probes. This method can introduce two transmission zeros on a linearly aligned substrate-integrated waveguide (SIW) resonant cavity, resulting in a fourth-order filter with quasi-elliptical response characteristics. However, this structure has a large radiation loss and a narrow bandwidth for the filter. Ref. [8] proposes a 6th-order cross-coupled filter that achieves negative coupling through slots on the top wide walls of the two resonant cavities. The filter introduces two transmission zeros and realizes a quasi-elliptical response. However, the filter's size is large and not easily scalable. In [9], a new implementation of a frequency-dependent coupling (FDC) structure is presented. This structure is composed of two coupled stepped-impedance grounded coplanar waveguides with open ends. A fourth-order linear hybrid electromagnetic coupling filter is designed using this structure. How-

ever, the filter only has one transmission zero and exhibits a large insertion loss. Ref. [10] presents a quasi-elliptic filter with controllable electric and magnetic mixed-coupling. The filter is based on substrate-integrated waveguide cavity resonators and uses a two-layer printed circuit board process. The design scheme combines an embedded short-ended strip line with a conventional inductive window between two cavities to create mixed coupling. This allows for separate control of electric and magnetic coupling by adjusting the width of the strip line and the inductive window. Additionally, a controllable transmission zero can be produced below or above the passband. However, this filter has a double-layer structure, which increases the filter's size and manufacturing difficulty. Refs. [11] and [12] introduce a transmission zero outside the passband of the filter through hybrid electromagnetic coupling between SIW resonant cavities. This extends the filter's stop-band width. However, the double-layer structure of this filter results in a larger size and higher insertion loss. In [13], two pairs of electrically mutually coupled uniform impedance resonators (UIRs) are etched between two rectangular SIW resonant cavities, realizing hybrid cross-coupling between the resonators and quasi-elliptical correspondence of the filter. However, the shape of this impedance resonator is complex, which increases its fabrication difficulty and limits its application. Ref. [14] describes a hybrid cross-coupling technique between resonators by integrating two quarter-wavelength microstrip resonators into two back-to-back quarter-mode substrate integrated waveguide (QMSIW) resonators. The resulting filter has four poles and two transmission zeros. However, the unique shape of the filter restricts its application to some ex-

\* Corresponding author: Wenjing Mu (muwenjing@gxun.edu.cn).

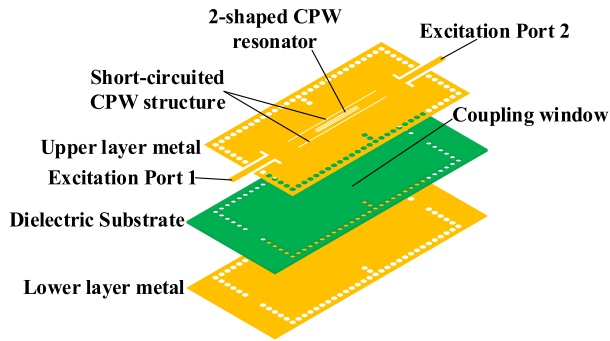


FIGURE 1. Structure of the filter.

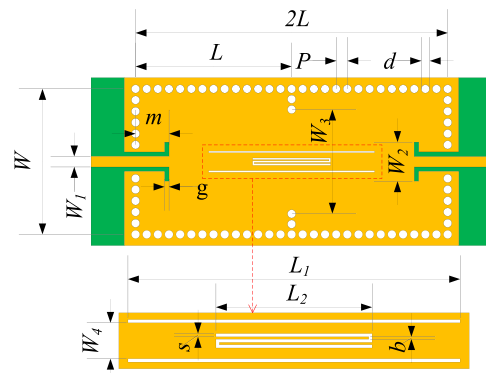


FIGURE 2. Dimensional drawing of the upper metal surface of the filter.

tent. Ref. [15] presents a SIW hybrid coupling filter based on through-silicon-via (TSV) technology. The filter is a second-order one-eighth mode SIW and has the advantages of being small and having low insertion loss. However, its transmission zero is too far away from the passband, making it less selective outside the passband. Ref. [16] proposes a SIW filter based on a silicon substrate. The filter is a quarter-mode (QM) and eighth-mode (EM) SIW filter. The filter adds a transmission zero out of band due to the electromagnetic hybrid coupling between the two resonators. However, the filter’s special shape restricts its application. In [17], a novel miniaturized bandpass filter (BPF) with high stopband rejection is proposed. The filter is based on a hybrid structure that employs QMSIW and microstrip technologies. This filter demonstrates flexible response with four poles and two controllable transmission zeros by integrating two quarter-wavelength microstrip resonators into two back-to-back QMSIW resonators. The filter is advantageous due to its small size and wide stopband. However, adjusting its transmission zeros is not easy.

The filters proposed in the literature have a problem achieving a comprehensive balance among several aspects, such as structural simplicity, low insertion loss, and flexible and controllable transmission zero positions. Based on the hybrid cross-coupling theory, this study presents a third-order filter with quasi-elliptical response characteristics. The filter is realized by etching two CPW structures within the upper metal surface of a second-order SIW resonant cavity. The proposed filter design scheme reduces complexity and provides excellent performance for potential applications.

## 2. STRUCTURE OF THE FILTER

The filter utilizes a substrate-integrated waveguide structure with a single layer. Figure 1 displays the three-dimensional structure of the filter, which consists of two metal layers and a dielectric layer. The dielectric layer is made of ZYF300CA-P, which has a relative permittivity of 3, a loss tangent of 0.0018, and a thickness of 0.762 mm. The filter has two SIW resonant cavities that operate in TE<sub>101</sub> mode. The resonant cavities are coupled through three components. The first component is an inductive coupling window, commonly used in the co-layer planar coupling design of SIW filters to provide magnetic coupling ( $M_C$ ). The second component is a short-circuited CPW struc-

ture with a length of approximately half a wavelength. Its end is connected to the center region of the two adjacent SIW resonant cavities to provide electrical coupling ( $E_C$ ). The third component is a 2-shaped CPW resonator with a length of approximately 1/4 wavelength. It is situated between the two SIW resonant cavities and the hybrid electromagnetic coupling structure and is isolated from the inductive coupling window. The coupling structure achieves hybrid cross-coupling in a linear manner, resulting in more transmission zeros and quasi-elliptical responses. Additionally, it reduces the filter’s design size. The filter’s input and output ports are constructed with coplanar waveguide transition structures to ensure impedance matching with the source or load. The dimensions of the upper metal surface of the filter are shown in Figure 2. To determine the dimensions of the filter, we first calculated the preliminary dimensions of the SIW resonator cavity based on the center frequency of the filter (4.5 GHz) and the dielectric constant of the substrate used. Then, we determined the preliminary dimensions of the short-circuited CPW structure and 2-shaped CPW resonator with respect to the wavelength. Finally, the filter was simulated and optimized using HFSS software to determine its final dimensions. Table 1 presents the final structural parameters of the filter after simulation and optimization using HFSS software.

TABLE 1. Structural parameters of the filter (unit: mm).

$L = 28$	$P = 2$	$d = 1.5$	$W = 26$
$m = 6$	$g = 0.8$	$W_1 = 1.88$	$W_2 = 7$
$W_3 = 18.72$	$W_4 = 3.2$	$L_1 = 29.8$	$L_2 = 14$
$s = 0.3$	$b = 0.2$		

## 3. FILTER DESIGN AND PRINCIPLE ANALYSIS

### 3.1. SIW Resonant Cavity Theory

The SIW is a waveguide-like structure that exhibits similar electromagnetic field transmission characteristics in the resonant cavity as a rectangular waveguide. However, the periodically spaced metalized vias in the sidewalls of the SIW prevent the current component from propagating in the longitudi-

nal direction, resulting in a radiation effect. Consequently, the transverse magnetic wave  $TM_{m0n}$  mode cannot propagate in the SIW. The SIW rectangular resonant cavity can only transmit  $TE_{m0n}$  modes, as the transverse electric wave  $TE_{m0n}$  mode has only a magnetic field component in the longitudinal propagation direction and no electric field component. The resonant frequency is given by Eq. (1):

$$f_{TE_{m0n}} = \frac{c_0}{2\sqrt{\varepsilon_r}} \sqrt{\left(\frac{m}{W_{eff}}\right)^2 + \left(\frac{n}{L_{eff}}\right)^2} \quad (1)$$

where  $c_0$  is the speed of light in vacuum;  $\varepsilon_r$  is the dielectric constant of the dielectric substrate;  $m$  and  $n$  are the number of modes along the width and length directions, respectively;  $w_{eff}$  and  $l_{eff}$  are the equivalent width and length of the SIW structure, which are defined as follows:

$$W_{eff} = W - \frac{d^2}{0.95P}, \quad L_{eff} = L - \frac{d^2}{0.95P} \quad (2)$$

The center distance between two rows of circular holes on the wide side of the cavity is denoted by  $W$ , the center distance between two columns of circular holes on the long side of the cavity denoted by  $L$ , the diameter of the circular holes denoted by  $d$ , and the circumcentric distance between adjacent circular holes denoted by  $P$ . To prevent electromagnetic energy from leaking out of the metal wall, it is necessary to satisfy the design rule of Eq. (3) when designing filters for various SIW structures.

$$d \leq \lambda/10, \quad P \leq 2d \quad (3)$$

The study's filter operates within the 5G FR1 band, with an initial resonant frequency of 4.5 GHz for the  $TE_{101}$  mode. Setting  $P = 2$  mm and  $d = 1.5$  mm, the dimensions of the cavity can be initially calculated according to Eqs. (1) and (2).

### 3.2. Hybrid Cross-Coupling Theory

Figure 3 shows the coupling topology of the filter, which includes three resonators. Resonators 1 and 3 are SIW resonators, while resonator 2 is a 2-shaped CPW resonator etched into the metal upper surface of the SIW resonator cavity. The coupling between the SIW resonators is a hybrid electromagnetic coupling. Magnetic coupling ( $M_C$ ) is provided by the inductive coupling window between the two SIW cavities, and electric coupling ( $E_C$ ) is provided by the short-circuited CPW structure with a length of approximately half wavelength. The coupling between the SIW resonator and 2-shaped CPW resonator is direct coupling.

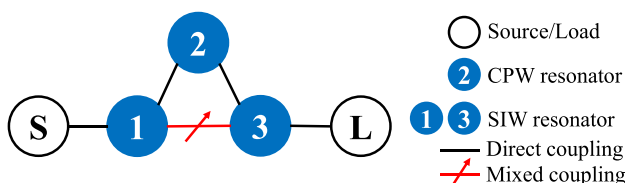


FIGURE 3. Coupling topology of the filter.

The coupling matrix of the filter can be expressed as:

$$\begin{bmatrix} 0 & M_{S1} & 0 & 0 & 0 \\ M_{S1} & M_{11} & M_{12} & M_{13}(\omega) & 0 \\ 0 & M_{12} & M_{22} & M_{23} & 0 \\ 0 & M_{13}(\omega) & M_{23} & M_{33} & M_{3L} \\ 0 & 0 & 0 & M_{3L} & 0 \end{bmatrix} \quad (4)$$

According to the theory of related literature [6], the position of the transmission zero point can be determined by the following equation:

$$\frac{M_{12} \cdot M_{23}}{M_{13}(\omega)} = \frac{1}{\text{FBW}} \left( \frac{\omega}{\omega_0} - \frac{\omega_0}{\omega} \right) \quad (5)$$

When the electric coupling coefficient  $E_C = 0$ , the hybrid cross-coupling coefficient can be expressed as:

$$M_{13}(\omega) = \frac{\omega M_{13}(\omega_0)}{\omega_0} \quad (6)$$

In the given equation,  $M_{13}(\omega_0)$  represents the coupling coefficient between resonances 1 and 3 when the input signal's angular frequency is the center angular frequency  $\omega_0$  of the filter. When the magnetic coupling coefficient  $M_C = 0$ , the hybrid cross-coupling coefficient can be expressed as:

$$M_{13}(\omega) = \frac{\omega_0 M_{13}(\omega_0)}{\omega} \quad (7)$$

When neither the electric coupling coefficient  $E_C$  nor the magnetic coupling coefficient  $M_C$  is zero, the hybrid cross-coupling coefficient can be expressed as:

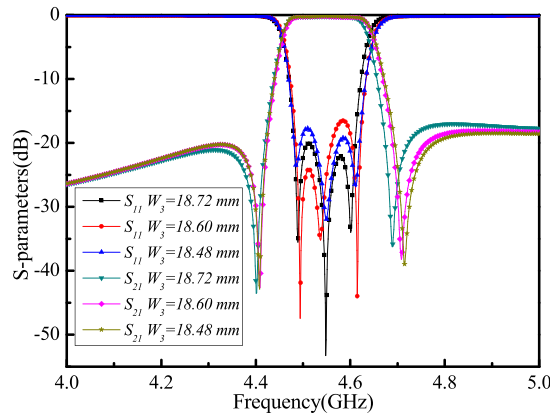
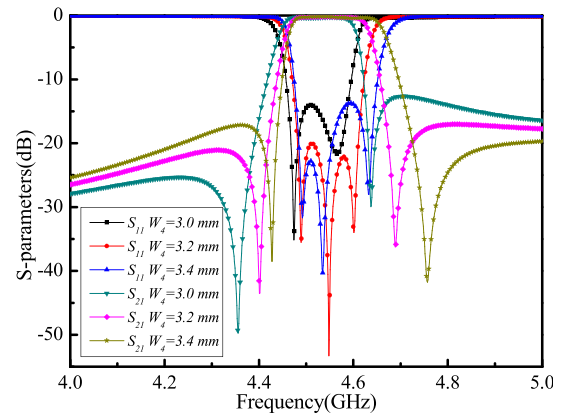
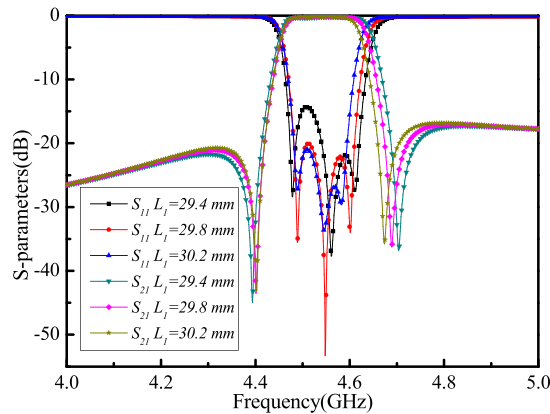
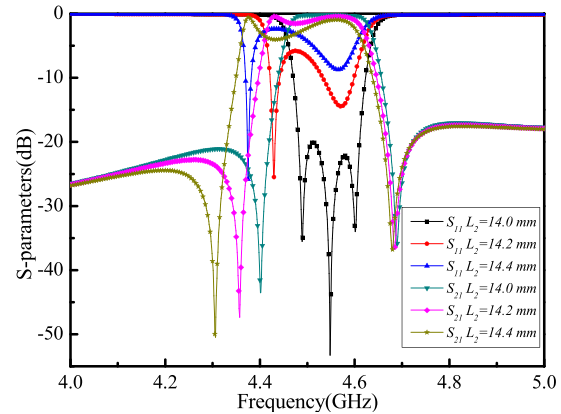
$$M_{13}(\omega) = \frac{\omega_0 M_{13}(\omega_0)(\omega^2 - \omega_m^2)}{\omega(\omega_0^2 - \omega_m^2)} \quad (8)$$

where FBW represents the relative bandwidth of the filter, and  $\omega_0$  and  $\omega_m$  represent the resonant frequency of the resonator and the frequency of the transmission zero point, respectively. If the cross-coupling is purely electric or magnetic, Eqs. (5), (6), and (7) indicate that only one transmission zero will be produced, which will appear on the left or right side of the pass-band. When both electric and magnetic couplings exist in cross-coupling, i.e., under the condition of mixed cross-coupling, the equation will produce two transmission zeros, as determined by Eqs. (5) and (8).

The filter's coupling matrix was extracted using the Couple-Fil software, based on its final  $S$ -parameter profile. The matrix is presented below:

$$\begin{bmatrix} 0 & 1.083 & 0 & 0 & 0 \\ 1.083 & 0 & 0.932 & 0.514/-0.489 & 0 \\ 0 & 0.932 & 0 & 0.932 & 0 \\ 0 & 0.514/-0.489 & 0.932 & 0 & 1.083 \\ 0 & 0 & 0 & 1.083 & 0 \end{bmatrix} \quad (9)$$

Based on the theory presented above, the filter structure proposed in this study can more effectively achieve a quasi-elliptic third-order filter with two transmission zeros.

FIGURE 4.  $S$ -parameter curves of the filter for different  $W_3$  dimensions.FIGURE 5.  $S$ -parameter curves of the filter for different  $W_4$  dimensions.FIGURE 6.  $S$ -parameter curves of the filter for different  $L_1$  dimensions.FIGURE 7.  $S$ -parameter curves of the filter for different  $L_2$  dimensions.

## 4. RESULTS AND ANALYSIS

### 4.1. Effect of $W_3$ Variation on Filter Performance

Figure 4 shows the  $S$ -parameter curves of the filter with varying  $W_3$  dimensions. The results indicate that decreasing the  $W_3$  size causes the transmission zero on the right side of the passband to shift towards higher frequencies more significantly than the transmission zero on the left side. As a result, the passband of the filter widens. The reduction of the size of  $W_3$  causes the magnetic coupling coefficient  $M_C$  in the hybrid cross-coupling to decrease, resulting in the above phenomenon. Therefore, adjusting the size of  $W_3$  can adjust the bandwidth of the filter and the position of the transmission zero on the right side of the filter.

### 4.2. Effect of $W_4$ Variation on Filter Performance

Figure 5 shows the  $S$ -parameter curves of the filter for different  $W_4$  sizes. It is evident that as the  $W_4$  size increases, both transmission zeros of the filter shift more significantly towards the high-frequency direction, resulting in a shift of the filter's passband towards the high-frequency direction. The phenomenon described above occurs because an increase in the size of  $W_4$  leads to an increase in the electric coupling coefficient  $E_C$  in the hybrid cross-coupling and a decrease in the inductive coupling window, which in turn causes a decrease in the magnetic cou-

pling coefficient  $M_C$  in the hybrid cross-coupling. As a result, adjusting the size of  $W_4$  allows for simultaneous adjustment of the position of the two transmission zeros of the filter and the position of the filter's passband.

### 4.3. Effect of $L_1$ Variation on Filter Performance

Figure 6 shows the  $S$ -parameter curves of the filter with varying  $L_1$  dimensions. The results indicate that increasing the  $L_1$  size causes the transmission zero on the right side of the passband to shift more significantly towards the low-frequency direction, while the transmission zero on the left side of the passband shifts less. This results in a narrower passband for the filter. The phenomenon described above occurs due to the increase in the size of  $L_1$ , which causes a decrease in the electrical coupling coefficient  $E_C$  in the hybrid cross-coupling. Therefore, adjusting the size of  $L_1$  allows for the adjustment of the position of the transmission zero on the right side of the filter and the bandwidth of the filter.

### 4.4. Effect of $L_2$ Variation on Filter Performance

Figure 7 shows the  $S$ -parameter curves of the filter with varying  $L_2$  dimensions. The transmission zero on the left side of the passband moves more significantly towards the low-frequency direction as the  $L_2$  size increases. Conversely, the transmission

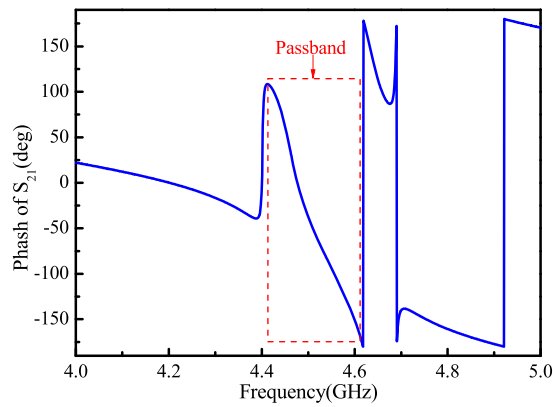


FIGURE 8. The phase characteristic curves of the  $S_{21}$  parameter.

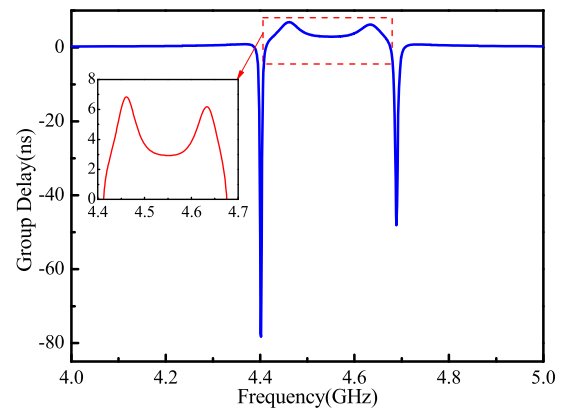


FIGURE 9. The group delay curve of the filter.

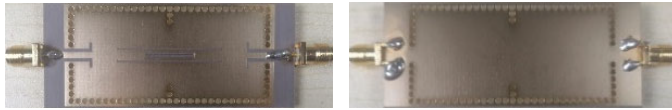


FIGURE 10. Physical picture of the filter.

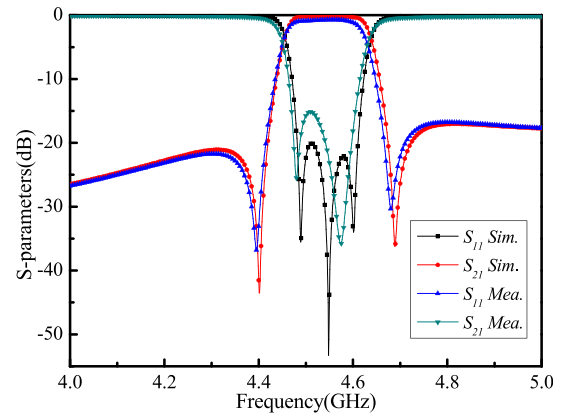


FIGURE 11. Simulation results and test results of the  $S$ -parameters of the filter.

zero on the right side of the passband moves less, resulting in a wider passband and poorer performance within the passband of the filter. The phenomenon described above occurs because the increase in the size of  $L_2$  reduces the resonance frequency of the 2-shaped CPW resonator. Therefore, adjusting the size of  $L_2$  allows for the adjustment of the position of the left transmission zero of the filter and the bandwidth of the filter.

#### 4.5. Group Time Delay Characterization and Phase Characterization of the Filter

Figure 8 displays the phase characteristic curves of the  $S_{21}$  parameter of the filter. It is evident that the linearity of the phase characteristic of the filter is superior in the passband. Figure 9 displays the group delay curve of the filter. It is evident that the group delay of the filter is less than 6.8 ns in the passband, and the maximum group delay variation is only 3.8 ns. At the same time, the filter exhibits a negative time delay at the transmission zeros, which is consistent with the characteristics of quasi-elliptical response filters.

#### 4.6. Test Results of the Filter

Based on the dimensions listed in Table 1, the physical filter underwent processing using the PCB method and is depicted in Figure 10. To conduct the physical test, SMA-KHD coax-

ial connectors must be soldered onto the input and output ports of the filter and then connected to an Agilent E8363C model network vector analyzer for measurement. The simulated and measured results of the  $S$ -parameters of the filter are presented in Figure 11. The measured and simulated  $S$ -parameter curves show a consistent overall trend. The filter has a center frequency of 4.55 GHz, a  $-3$  dB bandwidth of 180 MHz, a relative bandwidth of 4%, a return loss greater than 15 dB, and two transmission zeros located at 4.4 GHz and 4.69 GHz, respectively. The simulated insertion loss in the passband is approximately  $-0.4$  dB, and the measured insertion loss is 0.5 dB lower than the simulated value. The disparity between the measured and simulated values is primarily due to processing errors, dielectric loss, and conversion structure loss.

#### 4.7. Comparison with Similar Filters in the Literature

Table 2 compares the performances of the filter proposed in this paper with the SIW filters in references. The proposed filter exhibits advantages in terms of insertion loss, size, and controllability of transmission zeros. Additionally, the design methodology used is simple and easy to implement. The proposed hybrid cross-coupled structure can serve as a versatile and independent unit module. It not only is suitable for linear SIW filters but also

**TABLE 2.** Comparison with similar filters in the literature.

Refs.	Single layer	$f_0$ (GHz)	FBW (%)	Order	Insertion Loss (dB)	Size ( $\lambda_g^2$ )	TZ below, above $f_0$
[7]	✓	5.75	1.8	4	3.6	0.74	1, 1
[8]	✓	60	7.9	6	1.1	2.97	1, 1
[9]	✓	10	4.1	3	1.7	1.61	0, 2
[10]	×	27	7.4	4	2	2.43	1, 1
[11]	×	3.2	2.9	2	2.3	1.25	1, 0
[12]	×	3.7	1.7	2	2.3	1.31	0, 1
[13]	✓	8.8	6.1	4	2.2	1.39	1, 1
[14]	✓	10	22.7	4	1.2	0.85	1, 1
[15]	✓	9.9	18	2	0.88	0.62	1, 0
[16]	✓	10.7	35	2	0.7	0.78	0, 1
[17]	✓	10	22.7	4	1.2	0.37	1, 1
This work	✓	4.55	4	3	0.9	1	1, 1

can be applied to other topological forms of SIW filters, thereby enhancing their frequency selectivity.

## 5. CONCLUSION

This paper proposes a hybrid cross-coupling filter that utilizes a coplanar waveguide (CPW) resonator and a hybrid electromagnetic coupling structure. The filter is based on two CPW structures etched within the upper metal surface of a second-order substrate-integrated waveguide (SIW) resonant cavity. By adjusting the dimensions of the two CPW structures between the SIW resonant cavities and the width of the inductive coupling window, the strengths of the electric and magnetic coupling can be easily controlled to realize a controllable hybrid cross-coupling effect for tuning the position of the transmission zeros and ultimately realizing the third-order filter with the characteristics of a flexible and controllable position of the transmission zeros and a quasi-elliptical response property. Simulation and test results indicate that the filter has a center frequency of 4.55 GHz, a  $-3$  dB bandwidth of 180 MHz, a relative bandwidth of 4%, an insertion loss of  $-0.9$  dB in the pass-band, a return loss of over 15 dB, and two transmission zeros located at 4.4 GHz and 4.7 GHz, respectively. The filter has a simple structure, low insertion loss, a small circuit size, good frequency selectivity, and flexible and controllable transmission zeros. These advantages make it suitable for the use in 5G (sub-6 GHz) wireless communication systems.

## ACKNOWLEDGEMENT

This work is supported by the Chongzuo Science and Technology Program Project (No. 2023ZC1112), the School-level Research Project of Guangxi Minzu Normal University (No. 2022SP007), the Basic Research Ability Improvement Project for Young and Middle-aged Teachers in Guangxi Universities (No. 2023KY0793 and No. 2023KY0796), and the Guangxi Natural Science Foundation (No. 2022JJB150010).

## REFERENCES

- [1] Bozzi, M., A. Georgiadis, and K. Wu, "Review of substrate-integrated waveguide circuits and antennas," *IET Microwaves, Antennas & Propagation*, Vol. 5, No. 8, 909–920, Jun. 2011.
- [2] Chen, X.-P. and K. Wu, "Substrate integrated waveguide filter: Basic design rules and fundamental structure features," *IEEE Microwave Magazine*, Vol. 15, No. 5, 108–116, 2014.
- [3] Moscato, S., C. Tomassoni, M. Bozzi, and L. Perregini, "Quarter-mode cavity filters in substrate integrated waveguide technology," *IEEE Transactions on Microwave Theory and Techniques*, Vol. 64, No. 8, 2538–2547, Aug. 2016.
- [4] Jones, T. R. and M. Daneshmand, "Miniaturized folded ridged half-mode and quarter-mode substrate integrated waveguides for filter design," *IEEE Transactions on Microwave Theory and Techniques*, Vol. 67, No. 8, 3414–3426, Aug. 2019.
- [5] Qin, R., D. Zhang, Z. Ding, and M. Wang, "Duel-band filter with high out-of-band rejection using ACSRR-SIW technology," *IEICE Electronics Express*, Vol. 17, No. 12, 20190743, Jun. 2020.
- [6] Shen, W., L.-S. Wu, X.-W. Sun, W.-Y. Yin, and J.-F. Mao, "Novel substrate integrated waveguide filters with mixed cross coupling (MCC)," *IEEE Microwave and Wireless Components Letters*, Vol. 19, No. 11, 701–703, Nov. 2009.
- [7] Sirci, S., M. A. Sánchez-Soriano, J. D. Martínez, V. E. Boria, F. Gentili, W. Bösch, and R. Sorrentino, "Design and multiphysics analysis of direct and cross-coupled SIW combline filters using electric and magnetic couplings," *IEEE Transactions on Microwave Theory and Techniques*, Vol. 63, No. 12, 4341–4354, Dec. 2015.
- [8] Uemichi, Y., O. Nukaga, K. Nakamura, Y. Hasegawa, X. Han, R. Hosono, K. Kobayashi, and N. Guan, "A 60-GHz six-pole quasi-elliptic bandpass filter with novel feeding mechanisms based on silica-based post-wall waveguide," in *2017 IEEE MTT-S International Microwave Symposium (IMS)*, 1282–1284, Honolulu, HI, USA, 2017.
- [9] Liu, Q., D. F. Zhou, D. W. Zhang, and D. L. Lv, "A novel frequency-dependent coupling with flexibly controllable slope and its applications on substrate-integrated waveguide filters," *IEEE Microwave and Wireless Components Letters*, Vol. 28, No. 11, 993–995, Nov. 2018.

- [10] Gong, K., W. Hong, Y. Zhang, P. Chen, and C. J. You, "Substrate integrated waveguide quasi-elliptic filters with controllable electric and magnetic mixed coupling," *IEEE Transactions on Microwave Theory and Techniques*, Vol. 60, No. 10, 3071–3078, Oct. 2012.
- [11] Su, Z. L., B. W. Xu, S. Y. Zheng, H. W. Liu, and Y. L. Long, "High-isolation and wide-stopband SIW diplexer using mixed electric and magnetic coupling," *IEEE Transactions on Circuits and Systems II: Express Briefs*, Vol. 67, No. 1, 32–36, Jan. 2020.
- [12] Iqbal, A., J. J. Tiang, C. K. Lee, and B. M. Lee, "Tunable substrate integrated waveguide diplexer with high isolation and wide stopband," *IEEE Microwave and Wireless Components Letters*, Vol. 29, No. 7, 456–458, Jul. 2019.
- [13] Zhu, Y. and Y. Dong, "A compact dual-band quasi-elliptic filter based on hybrid SIW and microstrip technologies," *IEEE Transactions on Circuits and Systems II: Express Briefs*, Vol. 69, No. 3, 719–723, Mar. 2022.
- [14] Zheng, Y., Y. Zhu, Z. Wang, and Y. Dong, "Compact, wide stopband, shielded hybrid filter based on quarter-mode substrate integrated waveguide and microstrip line resonators," *IEEE Microwave and Wireless Components Letters*, Vol. 31, No. 3, 245–248, Mar. 2021.
- [15] Fan, C., X. Liu, Z. Zhu, and Y. Liu, "A compact eighth-mode SIW (EMSIW) filter with hybrid coupling based on TSV technology," in *2023 IEEE MTT-S International Microwave Workshop Series on Advanced Materials and Processes for RF and THz Applications (IMWS-AMP)*, 1–3, Chengdu, China, 2023.
- [16] Fan, C., X. Liu, Z. Zhu, Y. Liu, and Y. Yang, "A compact quarter-mode (QM) and eighth-mode (EM) substrate integrated waveguide (SIW) filter," in *2022 IEEE MTT-S International Microwave Workshop Series on Advanced Materials and Processes for RF and THz Applications (IMWS-AMP)*, 1–3, Guangzhou, China, 2022.
- [17] Zheng, Y., Y. Zhu, Z. Wang, and Y. Dong, "Compact, wide stopband, shielded hybrid filter based on quarter-mode substrate integrated waveguide and microstrip line resonators," *IEEE Microwave and Wireless Components Letters*, Vol. 31, No. 3, 245–248, Mar. 2021.